Phase behavior of Langmuir monolayers with ionic molecular heads: Molecular simulations

Carlos A. González-Castro and Guillermo Ramírez-Santiago
Departamento de Física-Química, Instituto de Física, Universidad Nacional Autónoma de México, Apartado Postal 20-364, México 01000, D.F., Mexico

(Received 29 May 2014; revised manuscript received 2 September 2014; published 16 March 2015)

We carried out Monte Carlo simulations in the N,Π,T ensemble of a Langmuir monolayer coarse-grained molecular model. Considering that the hydrophilic groups can be ionized by modulating acid-base interactions, here we study the phase behavior of a model that incorporates the short-range steric and long-range ionic interactions. The simulations were carried out in the reduced temperature range $0.1 \leqslant T^* < 4.0$, where there is a competition of these interactions. Different order parameters were calculated and analyzed for several values of the reduced surface pressure in the interval, $1 \leqslant \Pi^* \leqslant 40$. For most of the surface pressures two directions of molecular tilt were found: (i) towards the nearest neighbor (NN) at low temperatures, $T^* < 0.7$, and most of the values of Π^* and (ii) towards next-nearest neighbors (NNN) in the temperature interval $0.7 \leqslant T^* < 1.1$ for $\Pi^* < 25$. We also found the coexistence of the NN and NNN at intermediate temperatures and $\Pi^* > 25$. A low-temperature reentrant disorder-order-disorder transition in the positions of the molecular heads and in the collective tilt of the tails was found for all the surface pressure values. It was also found that the molecular tails arranged forming "rotating patterns" in the temperature interval, $0.5 < T^* < 1.5$, at intermediate surface pressures. We estimated the monolayer's surface pressure versus temperature and the temperature versus area per molecule phase diagrams. It was found that the LE $\leftrightarrow$ LC phase transition shifts to smaller temperatures when the molecular heads carry an ion in qualitative agreement with experimental observations of fatty acid monolayers with ionic head groups. Two surface pressure versus area per molecule isotherms were also calculated. At low temperatures near the LC-NN $\leftrightarrow$ LC-NNN transitions and at higher temperatures close to the LE $\leftrightarrow$ LC transitions. From these isotherms the monolayer's area compression modulus was obtained and its variation ranges in the LE and LC phases were found to be consistent with the experimental values.

DOI: 10.1103/PhysRevE.91.032409 PACS number(s): 68.18.−g, 68.35.Ct, 68.35.Rh, 82.20.Wt

I. INTRODUCTION

In the past decades a great deal of attention and effort has been focused to understand the structural properties and phase behavior of amphiphilic molecules deposited on a film. This research has been carried out from the experimental [1–13], theoretical [14–21], as well as from the molecular simulations [22–42] points of view. Amphiphilic molecules are formed by a hydrophilic ionic or polar head and a hydrophobic tail—usually one or more saturated alkane chains—that, when deposited on the surface of a fluid, form a monolayer. It has been found experimentally that the long-range repulsive interactions between molecular heads lead to the monolayer's rich structure and phase behavior. It is known that head-head interactions are modulated by partial dissociation when the subphase pH is varied [43–45]. For instance, in aqueous solutions of soaps with a pH between 7.0 and 10.0, the heads of long-chain fatty acids are partially ionized [12,43], while strong changes in the head-head interactions are expected when metal ions are present in the subphase [46–48]. It is known that fatty acids, phospholipids, and alcohols are formed by hydrophobic alkane chains with a similar molecular structure; however, the hydrophilic groups' molecular structure is what makes them differ [49]. It was found experimentally that the chains tilt directions occur either toward the nearest neighbor (NN) or toward the next-nearest neighbor (NNN). This orientational ordering was encountered over the temperature range, $0^\circ < T \leqslant 5^\circ$C. The NN phases occurred at low-surface-pressure values, whereas the NNN phases appeared at higher-surface-pressure values. The stability of the tilted phases observed in alcohol and fatty-acids molecules was related to the head-group interactions [50,51]. Nonetheless, the untilted phases found at higher surface pressures values were attributed to the chains interactions [49]. Experimental studies of fatty-acid monolayers with ionized molecular heads encountered that the phase boundaries shifted to lower temperatures [45]. It was also found that the phosphate hydration crucially affected the interfacial behavior of phospholipids deposited on the air-water interface [52].

The ionization of the head groups can be understood in terms of the acid-base interactions between hydrophilic groups. For instance, atomic force microscopy studies have provided a characterization of the electrostatic and acid-base interactions between hydrophilic self-assembled monolayers [53]. These studies involved monotropic ionizable acid functional groups ($COOH^-$) in aqueous solutions with different pH values. It was found that at low pH no-repulsive forces were detected as an indication that no-ionization and no specific ion binding occurred. However, as pH increased the acid groups dissociated and became negatively charged, reaching a maximum negative surface charge at pH $\geqslant$ 8.2 in pure water, that is, in the absence of electrolytes.

Experimental and molecular simulations studies have suggested that the monolayer's mean molecular area may be interpreted as a measure of both hydrocarbon chains packing and hydrophilic groups interactions. Among these interactions one can consider steric interactions (due to the volume requirements of the chains molecules and the molecular head groups), bonding interactions, and electrostatic interactions. Previous research has been aimed

at studying pattern formation and phase behavior due to dipolar interactions between the hydrophilic molecular heads [54,55]. Recently, the phase behavior of a coarse-grained molecular model (CGMM) of a Langmuir monolayer was investigated [56]. The amphiphilic molecules were modeled as rods with internal dipoles. It was found that in systems with low charge the melting transition was relatively independent of the charge strength and the tilting transition occurred at densities greater than the melting transition. However, at high dipole strengths the melting and tilting transitions were found to be coupled due to the existence of domains with collective tilt and increased hexagonal order at densities near the melting transition. Interestingly, the system underwent "frustration" due to the interplay between steric and dipolar interactions.

In this paper we present the results of Monte Carlo (MC) simulations of a version of the CGMM's of Langmuir monolayers developed previously [28–35]. In the present model we have incorporated the long-range interactions due to the Coulomb forces among the ionic hydrophilic molecular heads. Each molecular head carries a point charge, $q = -1$, at their center which is typically associated to the hydrophilic groups CH_2COO^-. Nonetheless, no attempt has been made to model a specific amphiphilic molecule. Our aim is to understand how the interplay between the steric interactions (van der Waals interactions) and the Coulomb interactions among the hydrophilic molecular heads affect the phase behavior of the monolayer. To this end we calculated several order parameters and the area per molecule as a function of temperature for several values of the surface pressure. Two surface-pressure-versus-area-per-molecule isotherms were also calculated and from them the area compression modulus was obtained. The outline of the paper is as follows: In Sec. II we describe briefly the CGMM and the details of the simulations. In Sec. III we explain briefly the order parameters we calculated to characterize the phase behavior of the system. In Sec. IV A some typical molecular configurations of the system with long-range interactions are shown and explained, and then in Sec. IV B the results for the behavior of the different order parameters at different surface pressure values are presented and analyzed. After this, in Sec. IV C, the phase diagrams surface pressure versus temperature and molecular area versus temperature are presented and discussed. Then in Sec. IV D two isotherms and the corresponding area compression modulus as a function of area per molecule are presented and discussed. Finally, a summary and the conclusions are given in Sec. V. The behavior of the enthalpy and the heat capacity as a function of temperature for different values of the surface pressure were also calculated and their behavior was related to the low- and high-temperature phase transitions of the system (see the Supplemental Material [57].)

II. MOLECULAR MODEL AND SIMULATIONS DETAILS

The monolayer's CGMM incorporates what are considered the most basic relevant interactions present in amphiphilic molecules deposited on a film. The aim is to reproduce the main features of the generic structure and phase behavior observed experimentally. Here we used the molecular model developed previously in a series of papers by the German group at Mainz [27–35]. For completeness, a brief explanation of the molecular potentials is given and their corresponding algebraic expressions are written down. The hydrophobic chains are mimicked by united effective beads, each representing two to three CH_2 groups, which are connected by nonlinear springs. The chain beads interactions are defined in terms of the truncated Lennard-Jones (LJ) potential, Eq. (1), with the restriction that interactions occur between every other monomer in the same chain molecule and through the nearest-neighbor beads among all the different chains:

$$V_T(r) = \begin{cases} \epsilon_T\left[\left(\frac{\sigma_T}{r}\right)^{12} - 2\left(\frac{\sigma_T}{r}\right)^{6}\right] - V_c, & \text{for} \quad r \leqslant r_c \\ 0 & \text{for} \quad r > r_c \end{cases}. \quad (1)$$

The value of V_c is chosen such that the potential is continuous at the cut-off radius, $r_c = 2\sigma_T$, and making tail beads attract each other. From now on, all the potentials parameters will be expressed as multiples of the LJ potential parameters, σ_T and ϵ_T. The nonlinear spring potential that represents the interaction between two contiguous beads in the same molecule is represented by the finite extended nonlinear elastic (FENE) potential,

$$V_B(q) = \begin{cases} -\frac{\kappa_B}{2} q_B^2 \ln\left[1 - \left(\frac{q-q_0}{q_B}\right)^2\right], & \text{for} \quad |q - q_0| < q_B, \\ \infty & \text{for} \quad |q - q_0| > q_B \end{cases}, \quad (2)$$

where the spring stiffness is $\kappa_B = 100\epsilon_T$, which ensures that the spring length fluctuations are sufficiently small in the temperature range of the simulations, and q_0 represents the position at which $V_B(q)$ is minimum and around which it is harmonic. The minimum of $V_B(q)$ has been chosen at $q_0 = 0.7\sigma_T$. This potential has a logarithmic cutoff at $q = q_0 \pm q_B$, with the bond length $q_B = 0.2\sigma_T$, the maximum displacement that a monomer can undergo. The bond "stiffness" potential between adjacent springs depends on the angle θ they form and is defined by

$$V_S(\theta) = \kappa_S(1 - \cos\theta) \quad (3)$$

with the stiffness constant, $\kappa_S = 10\epsilon_T$, measured in units of the tail-bead interaction strength, ϵ_T. Following Ref. [34] the molecular tails are allowed to submerge into the film surface up to a certain point at which they are repelled. To achieve this "hydrophobic interaction" a half of a FENE potential, $V_P(z)$, with strength, $\kappa_T = 10\epsilon_T$, between the tails beads and the film is introduced,

$$V_P(z) = \begin{cases} -\frac{\kappa_T}{2} z_{SP}^2 \ln\left[1 - \left(\frac{z_{0P}-z}{z_{SP}}\right)^2\right] & \text{for} \quad 2.5\sigma_T < z < 3.5\sigma_T, \\ 0 & \text{for} \quad 3.5\sigma_T < z. \end{cases} \quad (4)$$

with $z_{0P} = 3.5\sigma_T$ and $z_{SP} = \sigma_T$. In the simulations the film is located at, $z = 3\sigma_H$, to avoid negative values of the heads vertical positions which facilitates the implementation of the code. The hydrophilic molecular head groups are represented by effective beads with diameter, σ_H, and with a point electric charge at its center representing the ion. The steric interactions between head beads are represented by a truncated LJ potential with parameters ϵ_H, $\sigma_H = 1.2\sigma_T$ and a cut-off radius $r_c = \sigma_H$, such that head beads repel each other.

The long-range electrostatic interactions are represented by a full Coulomb potential, $U_C(r) = l_B T(q_1 q_2/r)$, with l_B the

Bjerrum's length. For pure water at $T = 300^\circ$ K, the Coulomb interactions are reduced in strength by a factor of about 80 relative to the vacuum; however, they maintain their long-range character. This reduction in the interactions strength is due to the permanent dipole moment carried by every water molecule since electrons tend to stay close to the oxygen, leaving two positively charged protons on the other side of the molecule. In the temperature range of the simulations, 293° K $\leqslant T \leqslant 303^\circ$ K, the Bjerrum length varies in the interval 6.9 Å $\lessapprox l_B \lessapprox$ 7.12 Å, that is, its variation is approximately $\Delta l_B \approx 0.22$ Å, about 3%. The typical lattice constant of a fatty acid in the LC phase with molecular tilt either towards the NN or the NNN may vary in the interval 4.773 Å $\lessapprox a_{\text{Latt.}} \lessapprox$ 5.413 Å [58]. Thus, the average distance between molecular heads in the condensed phase is about the same magnitude as the Bjerrum length. Therefore, there should be a competition between electrostatic and steric interactions in the temperature range of the simulations. As a consequence, both interactions play a role in the molecular heads' ordering.

Additionally, the molecular heads are subjected to a confining potential that restricts their vertical motion around the film's position. This is achieved by means of a half of a FENE potential with strength $\kappa_H = 10\epsilon_T$ that depends only on the hydrophilic molecular head vertical coordinate and is defined as

$$V_H(z) = \begin{cases} 0 & \text{for} \quad z < 2.5\sigma_H, \\ -\frac{\kappa_H}{2} z_{SH}^2 \ln\left[1 - \left(\frac{z - z_{0H}}{z_{SH}}\right)^2\right] & \text{for} \quad 2.5\sigma_H < z < 3.5\sigma_H, \end{cases} \tag{5}$$

with $z_{0H} = 2.5\sigma_H$ and $z_{SH} = \sigma_H$. Thus, the head beads are allowed to move in quasi three dimensions, that is, they can displace in the film's XY plane and undergo vertical motion within the slab, $2.5 < z/\sigma_H < 3.5$, above and below the film located at $z = 3$. Finally, the crossed interactions between chain beads and head beads are modeled using a LJ potential with parameters $\epsilon = \sqrt{\epsilon_T \epsilon_H}$ and $\sigma = \frac{1}{2}(\sigma_T + \sigma_H)$ according to the Lorentz-Berthelot mixing rules, with a cut-off radius $r_c = 1.1\sigma_T$, which makes the crossed interactions purely repulsive.

The MC simulations were performed following the same considerations as in references [30–35]. They were carried out in the isothermic-isobaric ensemble, N, Π, T, and MC moves were done by applying the Metropolis algorithm. The system basically consisted of $n = 144$ amphiphilic molecules each formed by seven beads including the head, making a total of $N = 7 \times n = 1008$ beads in the system. This number of molecules has proven to yield reasonable results in molecular simulations of Langmuir monolayers [38,40–42]. To estimate the significance of the finite-size effects in the results we carried out a few simulations on larger systems, $n = 256$ and 400 molecules, and found that they were not significant. However, no attempt has been done in carrying out a systematic finite-size analysis and we leave it for future work. The molecules are placed in a parallelepiped with sides (L_x, L_y, L_z) such that $L_x/L_y = 2/\sqrt{3}$ to allow for the hexagonal ordering of the head beads and $L_z \geqslant 7$. Periodic boundary conditions were applied along the X and Y directions and a shear deformation of the XY parallelogram by an angle, α, was introduced. It eliminates possible internal shear stress in the system that otherwise would introduce a symmetry breaking field that had an effect on the tilting phases and corresponding transitions in the system. A MC cycle consists of Nn MC moves each of these involves a single monomer displacement and a rescaling of the three coordinates that results in variations of L_x, L_y, and α. MC simulations were carried out in the reduced temperature range $0.10 \leqslant T^* < 4$, in steps of $\Delta T^* = 0.15$, and in the reduced surface pressure range $1 \leqslant \Pi^* \leqslant 40$ in steps of $\Delta\Pi^* = 5$. These reduced quantities are defined as $T^* = (k_B/\epsilon_T)T$ and $\Pi^* = (\sigma_T^2/\epsilon_T)P$. The temperature and surface pressure intervals considered here correspond to the following actual ranges: $20 \leqslant T \leqslant 30$ (in degrees Celsius) and $1 < \Pi < 70$ mN/m. For reasons of space and simplification, from now on we will refer to the reduced temperature and reduced surface pressure simply as temperature and pressure.

The experimental surface pressure is a force acting upon a unit length of the barrier separating the pure surface of a liquid and the surface of the same liquid covered with an adsorption layer of a surfactant. Because of this it is given by the surface tensions difference: $\Pi(A,T) = \gamma_o(A,T) - \gamma_m(A,T)$, where $\gamma_o(A,T)$ is the surface tension of the pure liquid and $\gamma_m(A,T)$ is the monolayer surface tension. Nonetheless, for the model considered here the aqueous subphase is represented by a confining external potential, $V_H(z)$ [Eq. (5)], and the intermolecular pressure tensor was calculated as [30,56,59]

$$\Pi_{\alpha,\beta}(A,T) = \frac{Nk_BT}{A}\delta_{\alpha,\beta} + \frac{1}{A}\left\langle \sum_{i=1}^{N} r_{i\alpha} F_{i\beta} \right\rangle. \tag{6}$$

The sum was carried out over all beads and α, β denote the coordinates x and y, while $\vec{F}_i$ represents the force acting upon the i-th bead. Since the simulation two-dimensional box was of variable shape the pressure tensor became diagonal as an indication that no internal stress was present in the monolayer. At mechanical equilibrium, according to the virial theorem the surface pressure is obtained as $\Pi_{\alpha,\beta}(A,T) = \Pi(A,T)\delta_{\alpha,\beta}$.

To equilibrate the system at high temperatures and low surface pressures were required of the order of 10^6 MC cycles. Averages of the quantities of interest were calculated over 600 blocks, each consisting of 500 MC cycles. Nonetheless, at low temperatures and high surface pressures the system reached equilibrium after 1.5×10^6 MC cycles and the corresponding averages were calculated over 1000 blocks, each having 500 MC cycles. To obtain a smoother behavior in the quantities of interest we interpolated three points between two consecutive simulated temperatures.

Although the Ewald summation approach used to evaluate the long-range electrostatic interactions formally requires an electric charge neutralization condition, it can also be applied to a charged system as well. In this latter situation, the omission of the $k = 0$ term in the Fourier transform of the real-space charge density introduces a uniform background charge density in the box, which effectively neutralizes the system. This causes a uniform shift in the real space charge density, upon back transformation from Fourier space, that is, $\rho\prime(\vec{r}) = \rho(\vec{r}) - \sum_{i=1}^{N} q_i / V_{\text{box}}$, with V_{box} the volume of the central simulational box. In such a case a correction term is required to account for the interactions between the

point charges and the background charges in the real space sum [60]. This is achieved by shifting the electrostatic energy by $V = -(\pi/2\alpha^2)(\sum_{i=1}^{N} q_i)^2/V_{\text{box}}$, with α the Ewald splitting parameter. When averaged over the box volume, the Ewald potential is zero. This correction term also ensures that the potential energy of the charged system becomes independent of the choice of the value of α. Because the background charge is uniformly distributed and does not exert a force on charged particles it is considered an acceptable countercharge distribution [61]. For a recent review on this topic see Ref. [62].

III. ORDER PARAMETERS

The order parameters are quantities related to the system symmetries and degrees of freedom, thus their behavior yields information on the positional ordering of the molecular heads as well as on the orientational ordering of the molecular tails. To this end we calculated and analyzed in detail the behavior of the following order parameters: Ψ_6, K_{nn}, and R_{xy}, which are defined below. To complement the analysis we also calculated the molecular average tilt, $\langle[\theta]\rangle$, the area per molecule, A/n, as well as the product, $(A/n)\cos\theta$. The two-dimensional melting hexagonal order parameter, ψ_6, is related to the positional ordering of the head beads. It measures the long-range orientational order of the nearest-neighbor directions and is defined as

$$\psi_6 = \left\langle \left| \frac{1}{6N} \sum_{j=1}^{N} \sum_{k=1}^{6} e^{6\imath\phi_{jk}} \right|^2 \right\rangle, \tag{7}$$

where ϕ_{jk} represents the angle formed by the vector that joins two contiguous head beads and a given reference direction. The index j runs over all the N head beads and the index k runs over the six nearest neighbors of a given head bead. This order parameter is equal to zero when the molecular heads positions are randomly located and is equal to 1 when they are located on the vertices of a perfect hexagonal lattice. The order parameter K_{nn} measures the orientational correlations between nearest-neighbor molecular tails. It is zero when the molecular tails are randomly oriented and equal to 1 when all the tails are oriented in an specific direction. It is defined as

$$K_{nn} = \left\langle \frac{1}{6n} \sum_{j=1}^{n} \sum_{k=1}^{6} \frac{1}{2}[3\cos^2(\theta_{jk}) - 1] \right\rangle, \tag{8}$$

where θ_{jk} is the angle between the director vectors of two nearest-neighbor molecules. The index k runs over the six nearest-neighbor head beads and the j runs over all the n molecules in the system. The order parameter, R_{xy}, is related to the molecular collective tilt and represents the average of the projection of the director vector, $\vec{D}_i$, over all molecules in one system configuration. The vector $\vec{D}_i$ goes from the head bead to the last tail bead of each molecule. It is defined as

$$R_{xy} = \sqrt{\langle [x]^2 + [y]^2 \rangle}, \tag{9}$$

where the quantity $[x]$ ($[y]$) represents the average over all molecules in one system configuration of the x (y) component of the director vector, $\vec{D}_i$. The triangular brackets denote the statistical average over the different system configurations. The molecular average tilt, $[\theta]$, is calculated as the average over all molecules—in one system's configuration—of the angle θ_i that forms the director vector of each molecule with the XY plane. This quantity is not related to the azimuthal symmetry breaking, so it differs from zero even in the untilted LC phase. Nevertheless, the thermal average, $\langle[\theta]\rangle$, over all configurations exhibits a sharp kink at the tilting transition. The monolayer's mean molecular area, A/n, is amenable to be measured experimentally. Finally, the product, $(A/n)\cos\theta$, is directly related to the total volume occupied by the monolayer.

IV. RESULTS

To be able to compare and better understand the behavior of the different order parameters and phase diagrams of the system of interest we include the results for a monolayer in which the molecular heads carry an ion, referred to as system A, and a monolayer in which the molecular heads carry no ion, referred to as system B. The analysis for system B has already been carried out in Refs. [33,34]. To get an intuitive picture of the molecular arrangements in the different phases we begin this section by presenting eight representative molecular configurations obtained from the MC simulations.

A. Molecular configurations

To investigate the ordering of the ionic molecular heads we constructed the Voronoi polygons with their positions. It is known that when the molecular heads are positioned at the sites of a hexagonal lattice the Voronoi construction yields perfect hexagons. In Fig. 1 are shown four molecular configurations with the corresponding Voronoi polygons that were obtained from system A's configurational snapshots for the surface pressure and temperature values indicated below. The circles represent the hydrophilic heads while the segments represent the projections of the molecular tails onto the XY plane. The line segments at the box edges correspond to the molecular tails after periodic boundary conditions were applied. The top left panel represents a molecular configuration obtained for $\Pi^* = 1$ and $T^* = 0.70$, where the molecular heads are positionally disordered and the molecular tails point towards their NN. The top right panel shows a molecular configuration obtained for $\Pi^* = 1$ and $T^* = 0.40$, where the molecular heads are positionally disordered and the molecular tails point towards their NNN. The bottom left panel corresponds to a molecular configuration obtained for $\Pi^* = 15$ and $T^* = 1.15$, and in this case the molecular heads arrange closely in a hexagonal lattice, whereas the molecular tails point towards their NNN. The bottom right panel represents a molecular configuration obtained for $\Pi^* = 5$ and $T^* = 0.55$, where the molecular heads are positionally ordered in a hexagonal lattice while there are regions where the molecular tails point towards their NN (right-side region) and other regions where they orient towards their NNN (intermediate upper region). That is, there appears to be a coexistence of the subphases NN and NNN, which is represented as NN(N).

In Fig. 2 are also shown another four different molecular configurations for different surface pressure and temperature values. The top left panel shows the configuration obtained for $\Pi^* = 10$ and $T^* = 0.10$. There it is seen that the molecular heads are positionally disordered while the molecular tails

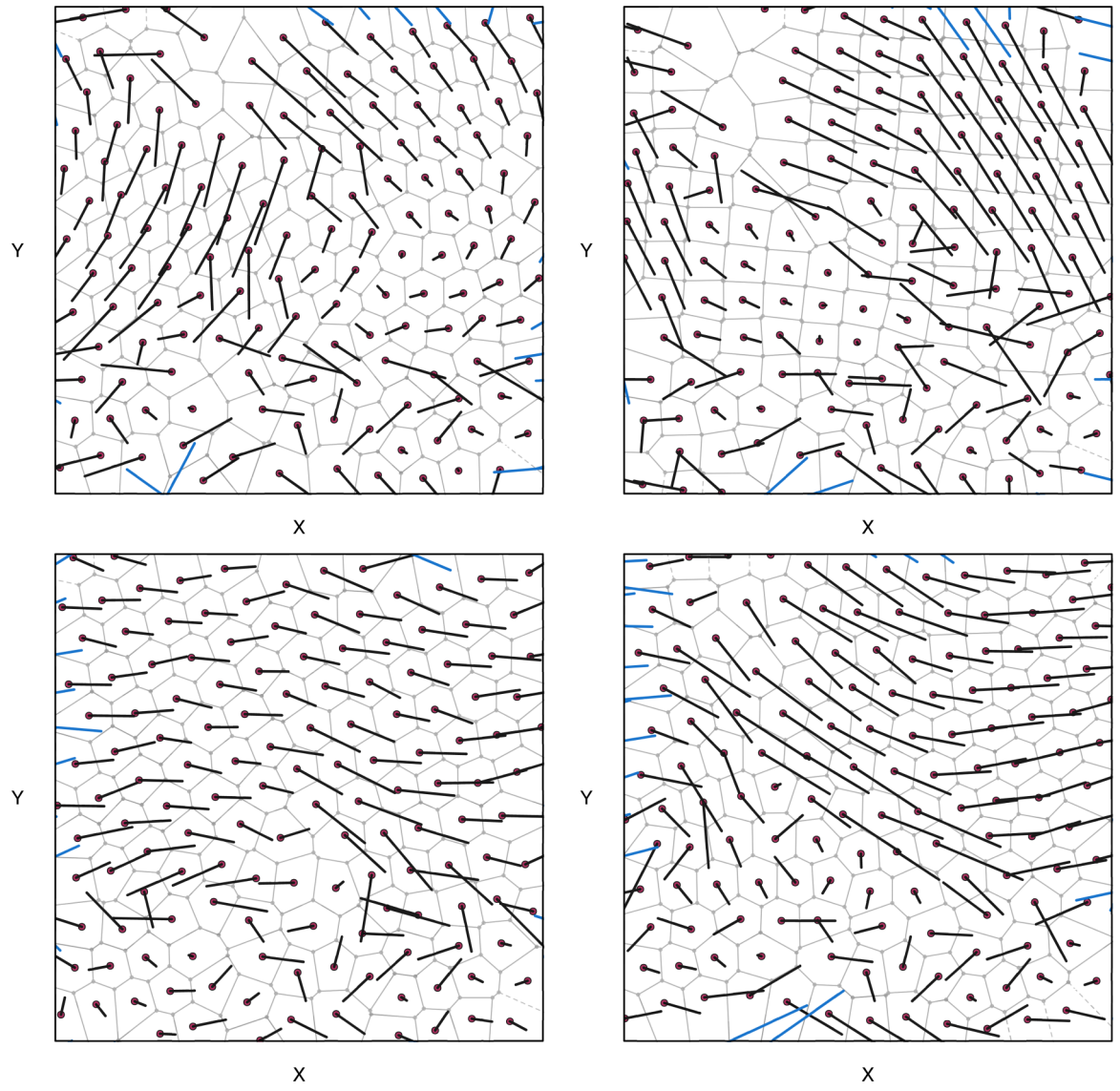

FIG. 1. (Color online) Molecular configurations and Voronoi polygons for the monolayer with ionic molecular heads. Top left panel: $\Pi^* = 1$ and $T^* = 0.70$; molecular heads are positionally disordered while some molecular tails point towards their NN. Top right panel: $\Pi^* = 1$ and $T^* = 0.40$; molecular heads are positionally disordered while the molecular tails point towards their NNN. Bottom left panel: $\Pi^* = 15$ and $T^* = 1.15$; molecular heads arrange closely in a hexagonal lattice and the molecular tails point towards their NNN. Bottom right panel: $\Pi^* = 5$ and $T^* = 0.55$; molecular heads are positionally ordered in a hexagonal lattice while there are regions where the molecular tails point towards their NN (right-side region) and other regions where they orient towards their NNN (intermediate upper region). This molecular arrangement may suggest the coexistence of the subphases NN and NNN.

are disordered since they point in different directions. In the top right panel is shown the configuration obtained for $\Pi^* = 15$ and $T^* = 0.10$. As in the previous panel, it is seen that the molecular heads are positionally disordered while the molecular tails are disordered since they point in different directions. In the bottom left panel it is shown a "vortex pattern" formed with the molecular tails when the system is at the surface pressure value $\Pi^* = 10$ and at the temperature $T^* = 0.70$. In this case the molecular heads appear to be positionally ordered at the vortex center. Finally, the bottom right panel shows a molecular configuration when the surface pressure value $\Pi^* = 30$ and at the temperature value $T^* = 1.15$. It is seen that most of the molecular heads are positionally ordered and located in a hexagonal lattice, whereas the majority of the molecular tails are in a vertical position. In the following subsection the order parameters behavior is presented and analyzed.

B. Order parameters

By carefully analyzing the behavior of the order parameters K_{nn}, Ψ_6, R_{xy} and the quantities $\langle[\theta]\rangle$, A/n (area per molecule), as well as the product $(A/n)\cos\theta$ as functions of temperature for several values of the surface pressure, the phase transitions in the orientation of the molecular tails and in the positions of the molecular heads were located. By definition an order parameter is greater than zero in the ordered phase, whereas it is equal to zero in the disordered phase. However, due to the

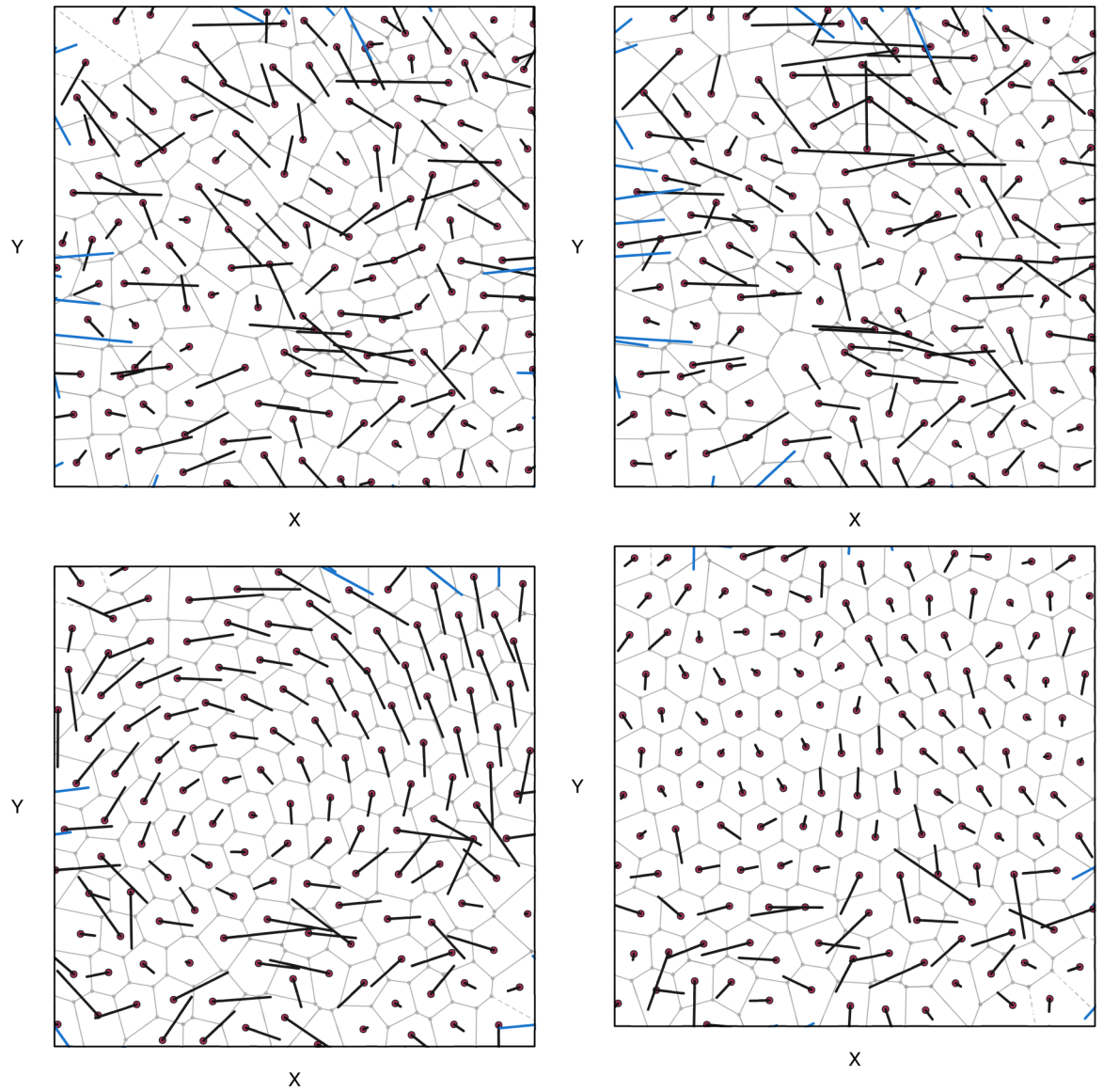

FIG. 2. (Color online) Molecular configurations and Voronoi polygons for the monolayer with ionic molecular heads. Top left panel: $\Pi^* = 10$ and $T^* = 0.10$; molecular heads are positionally disordered while the molecular tails show no orientational order at all. Top right panel: Similar molecular configurations as in previous panel but for different values of the surface pressure and temperature: $\Pi^* = 15$ and $T^* = 0.10$. Bottom left panel: Molecular tails arrange in a vortex pattern while the molecular heads at the vortex center appear to be positionally ordered. This configuration was obtained for $\Pi^* = 10$ and $T^* = 0.70$. Bottom right panel: Most of the molecular heads are positionally ordered to form a hexagonal lattice while some of the molecular tails are vertical for $\Pi^* = 30$ and $T^* = 1.15$.

finiteness of the simulated system the order parameters usually fluctuate in the disordered phases, either about zero or about a number close to zero. In addition, they are smeared out at their rise as the transition is approached from the disordered phase. This is the kind of behavior that was obtained for the order parameters and related quantities calculated here.

It is expected that upon lowering the temperature at the LE-LC phase transition the molecular heads tend to arrange in a hexagonal lattice. Simultaneously, there occurs the rodlike alignment of the molecular tails which in turn leads to an increase of the orientational correlations. Because of this, we start by presenting the order parameters Ψ_6 and K_{nn} that account for these changes. Figures 3(a)–3(d) show the results for these quantities for systems A and B. For system A, Figs. 3(a) and 3(c), for $T^* > 2.5$, before the LE-LC phase transition takes place, Ψ_6 fluctuates in the interval $0 < \Psi_6 \leqslant 0.2$. Upon decreasing further the temperature and when the LE-LC transition is approached, Ψ_6 rises and its value increases since the molecular heads become positionally ordered, forming a hexagonal lattice. As pressure increases the LE-LC phase transition shifts to higher temperatures. In addition, the values that Ψ_6 reaches as it rises from zero shift up and down as pressure varies, behavior that may be ascribed to the softening of the hexagonal lattice. In the LC phase, Ψ_6 attains smaller values for system A than those it reaches for system B, as shown in Fig. 3(b). For system A it is found that, when $T^* \lessapprox 0.4$, Ψ_6 drops suddenly, suggesting a reentrant order-disorder-like behavior in the molecular heads

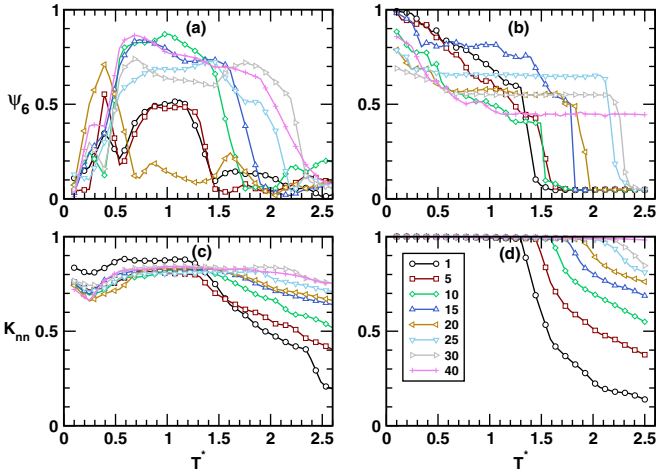

FIG. 3. (Color online) Behavior of Ψ_6, and K_{nn} as a function of temperature and different surface pressure values for a monolayer with ionic molecular heads (left panels) and for a monolayer with nonionic molecular heads (right panels).

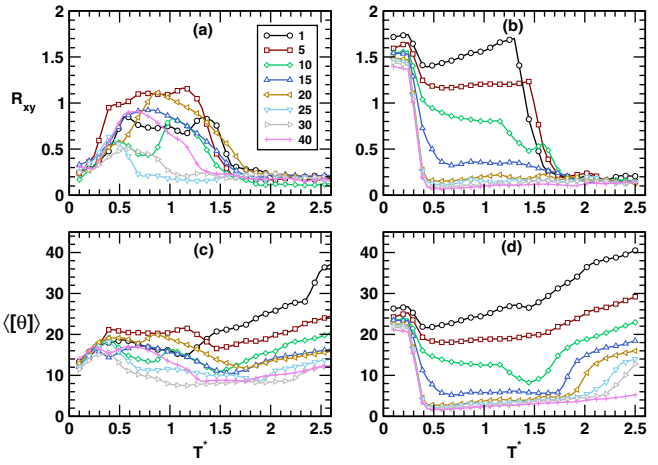

FIG. 4. (Color online) Behavior of R_{xy} and $\langle[\theta]\rangle$ (in degrees) as a function of temperature and different surface pressure values for a monolayer with ionic molecular heads (left panels) and for a monolayer with nonionic molecular heads (right panels).

positions. Since this kind of behavior is not observed for system B this transition is then due to the Coulomb interactions between molecular heads. With regard to the orientational correlation function, K_{nn}, it is found that upon decreasing the temperature it increases almost monotonically such that the higher the pressure the higher its values but with a flatter slope. Nonetheless, the values of K_{nn} for system A are smaller than those obtained for system B. See Fig. 3(d). Unlike for system B, as the LE-LC phase transition is approached, the rise of K_{nn} smears out and this spreading becomes larger as pressure increases. At intermediate temperatures, in the LC phase, K_{nn} becomes almost flat. Upon lowering further the temperature a small dip is observed at about the same temperature where Ψ_6 drops its value. This suggests that some kind of reentrant transition is also happening in the orientation of the molecular tails, as will be confirmed below, when the behavior of the collective tilt is analyzed. In Figs. 3(b) and 3(d), the quantities Ψ_6 and K_{nn} are plotted for system B. As expected, the LE phase occurs at high temperatures where these quantities attain small values. Upon lowering further the temperature the LE-LC phase transition is reached and a sharp rise in both quantities occurs at about the same temperatures for each pressure value. In Fig. 3(d) it is also observed that the higher the pressure the smaller the increase in K_{nn} since it has a flatter slope. As pressure increases the LE-LC transition temperatures shifts to higher values in the interval, $1.4 \lessapprox T^* \lessapprox 2.4$, except for $\Pi^* = 40$, in which case the LE-LC transition occurs for $T^* > 2.5$. In addition, the values that Ψ_6 reaches as the system passes the LE- LC phase transition fluctuate as pressure varies. For pressures in the range $1 \leqslant \Pi^* \leqslant 20$, these fluctuations are in the interval $0.45 \lessapprox \Psi_6 \lessapprox 0.55$. For $\Pi^* = 25$, it increases up to $\Psi_6 \approx 0.65$, and for $\Pi^* = 30$ and 40 it decreases to the initial interval. This behavior may be ascribed to the softness of the hexagonal lattice. In the LC phase Ψ_6 increases monotonically as temperature decreases, although there are still some fluctuations its overall values become higher as pressure increases from $\Pi^* = 1$ up to $\Pi^* = 10$.

Let us now turn to the collective molecular tilt that is quantified by R_{xy}, and the average molecular tilt $\langle[\theta]\rangle$. Their behavior is shown for systems A and B in Figs. 4(a)–4(d) and is analyzed simultaneously since both quantities yield information about the orientational ordering of the molecular heads. For system A, the collective tilt fluctuates about $R_{xy} \lessapprox 0.25$ for $T^* > 1.8$. Upon decreasing the temperature the LE-LC phase transition is reached and R_{xy} rises as an indication that the molecular collective tilt takes place. The temperatures at which R_{xy} rises moves slightly to lower temperatures as pressure increases from $\Pi^* = 1$, 5, to 10. Increasing further the pressure, from $\Pi^* = 15$ to 20, the transition temperatures shift to higher values. For higher pressures, $\Pi^* = 25$, 30, and 40, the transition temperatures move back again to lower values. The lowest temperature at which R_{xy} rises occurs for $\Pi^* = 25$, and then it increases for $\Pi^* = 30$ and 40. This shifting in the temperatures may be related to the existence of the LC-NN and the LC-NNN subphases, as suggested by a careful analysis of molecular configurations snapshots. For system B a similar shifting in the temperatures at which R_{xy} rises is observed for $15 \leqslant \Pi^* \leqslant 40$, as can be seen in Fig. 4(b). For system A, however, R_{xy} shows a monotonic decrease at low temperatures and it drops to a value $R_{xy} \approx 0.2$ at $T \lessapprox 0.3$, suggesting that an order-disorder reentrant-like behavior in the collective molecular tilt takes place. This reentrant-like behavior at low temperatures is consistent with that found for the molecular heads order parameter Ψ_6. Because of the Coulomb interactions the hexagonal lattice softens sufficiently and deforms such that the molecular tails have more room to wiggle around, leading to a decrease in the correlations of the collective molecular tilt. Unlike for system A, the overall behavior of R_{xy} for system B is plotted in Fig. 4(b). It suggests that there are two temperature regimes: (i) at high temperatures, $T^* \gtrapprox 1.6$, where $R_{xy} \approx 0.15$, for $\Pi^* = 1$, 5,10, and 15, as an indication that the LE phase sets in, and (ii) at low temperatures, $R_{xy} > 0.15$, due to the establishment of the LC phase. However, the low-temperature behavior of R_{xy} shows no signature of a low-temperature order-disorder reentrant

transition. It was also found that the temperatures at which R_{xy} rises moves slightly to higher values as pressure increases from $\Pi^* = 1$, 5, 10, and 15. However, for $\Pi^* = 20$, 25, 30, and 40, the rise in R_{xy} takes place at about $T^* \approx 0.4$, right at the LC phase. This behavior can be related to the existence of the LC-NN and LC-NNN subphases [33]. Certainly, the LC-U phase should occur at even lower temperatures and higher surface pressure values, $\Pi^* > 40$.

With regard to the molecular tail's average tilt, $\langle[\theta]\rangle$, plotted in Fig. 4(c) for system A, it decreases slowly upon decreasing the temperature until it reaches a minimum. The position of this minimum shifts to higher temperatures as pressure increases in the interval $5 \leqslant \Pi^* = 1 \leqslant 25$. Nonetheless, for $\Pi^* = 30$ and 40, the location of the minimum moves back to lower temperatures. For $T^* > 1.8$, the overall values of $\langle[\theta]\rangle$ become smaller as pressure increases. Lowering further the temperature the average tilt increases and reaches two maxima for all the values of Π^*. These maxima are related to the existence of the LC-NN and LC-NNN subphases, as it happened for R_{xy} and as suggested by a careful analysis of molecular configurations. In addition, the overall values that $\langle[\theta]\rangle$ reaches at intermediate temperatures oscillate as surface pressure varies. At temperatures $T^* \lessapprox 0.5$, the molecular average tilt decreases monotonically until it reaches its lowest value, $\langle[\theta]\rangle \gtrapprox 11\,^{\circ}$, suggesting that, on average, the molecules show some tilting. Thus, for system A the overall behavior described for $\langle[\theta]\rangle$ is fully consistent with the one described for the collective molecular tilt, R_{xy}. The behavior of $\langle[\theta]\rangle$ for system B is shown in Fig. 4(d). In this case its overall values become smaller upon increasing the pressure in the full temperature range studied. Upon decreasing the temperature from $T^* = 2.5$, it is seen that $\langle[\theta]\rangle$ decreases slowly for most of the pressure values except for $\Pi^* = 40$, in which case the average tilt is almost flat until it reaches the temperature $T^* \approx 0.45$. For $\Pi^* = 1$ and 5 the average tilt develops two inflection points, in the former at $T^* \approx 2.1$ and $T^* \approx 1.5$ while in the latter at $T^* \approx 2$ and $T^* \approx 1.5$. These inflection points signal the transition from the gas phase to the coexistence of the gas-LE phases and the LE-LC phase transition, respectively. For higher pressures, $\langle[\theta]\rangle$ is almost flat in the temperature interval $0.5 \leqslant T^* \lessapprox 2$. At the temperature $T^* \approx 0.5$ the average tilt rises suddenly for all the pressure values as an indication that the molecular tilt occurs in a particular direction, towards the NN, that is, the LC-NN subphase establishes.

In Figs. 5(a)–5(d) the results for A/n and the product, $(A/n)\langle\cos(\theta)\rangle$, are plotted for systems A and B. For system A the gas phase can be identified by the high values of the area per molecule, $A/n \approx 5$, that occur at low pressures, $\Pi^* \leqslant 1$, and high temperatures, $T^* \gtrapprox 3.5$. For system B the gas phase is identified for values of the area per molecule, $A/n \lessapprox 3$, and it occurs for pressures $\Pi^* \leqslant 1$ and temperatures $T^* \gtrapprox 2.5$. At lower temperatures, in the interval $2.4 \leqslant T^* < 3.5$ and $\Pi^* = 1$, the area per molecule for system A decreases and takes values in the interval $1.8 < A/n < 5$. Nonetheless, for system B it happens in the temperature interval $1.5 \leqslant T^* < 2.5$. This behavior suggests in both cases the coexistence of the gas and LE phases. For system A both quantities develop inflection points at $T^* \approx 3.5$, 2.4 and $T^* \approx 1.4$. The high-temperature one is related to the LE-gas phase transition while the intermediate-temperature inflection points indicate the passing

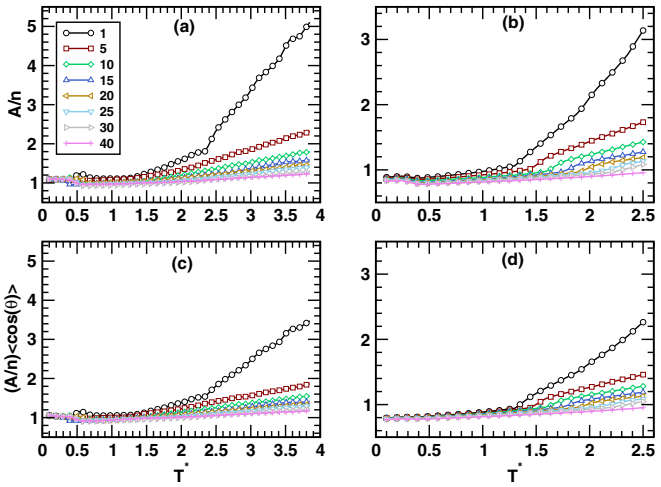

FIG. 5. (Color online) Behavior of A/n and $A\cos(\theta)/n$ as a function of temperature and different surface pressure values for a monolayer with ionic molecular heads (left panels) and for a monolayer with nonionic molecular heads (right panels).

of the system from the gas-LE coexistence to the full LE phase. The low-temperature inflection point signals at the LE-LC phase transition. However, for system B a smooth decrease of both quantities is observed in the temperature interval $1.3 \leqslant T^* < 2.5$. At $T^* \approx 1.3$ the LE-LC phase transition is signaled by the change in the slope of both quantities. Nonetheless, it is found for both systems that the higher the value of the pressure the smaller the slope with which these quantities decrease upon lowering the temperature. It should also be noted that at high temperatures, before the LC phase sets in, the product, $(A/n)\langle\cos(\theta)\rangle$, is smaller than the area per molecule, A/n, for both systems. This happens because in the LE phase the molecular chains tilting are uncorrelated, that is, $\langle\cos(\theta)\rangle < 1$. On the other hand, for system A, the low-temperature behavior ($T \lessapprox 0.5$) of these quantities is such that they undergo a small increase for $\Pi^* > 1$ and a small bump occurs for $\Pi^* = 1$, suggesting the existence of a phase transition. This behavior is fully consistent with the reentrant order-disorder transition in the positions of the molecular heads and in the orientation of the molecular tails. In contrast, for system B, a very small increase in A/n is observed at $T^* \approx 0.25$, which may be related to a small deformation of the molecular heads hexagonal lattice. However, the reentrant-like behavior observed in A/n for system A is not seen in the quantity $(A/n)\langle\cos(\theta)\rangle$, and, instead, it shows a flat behavior at low temperatures, $T^* \lessapprox 0.3$. That is, the reentrant-like behavior that happens in system A does not change the monolayer volume; however, it does change A/n, since it is interpreted as a measure of the molecular chains packing and hydrophilic interactions.

C. Phase diagrams

In this section we present the phase diagrams Π^* versus T^* and T^* versus A/n for systems A and B. They were obtained from a detailed analysis of the order parameters. To cross-check the location of the phase transitions the temperature positions of the maxima and minima of the

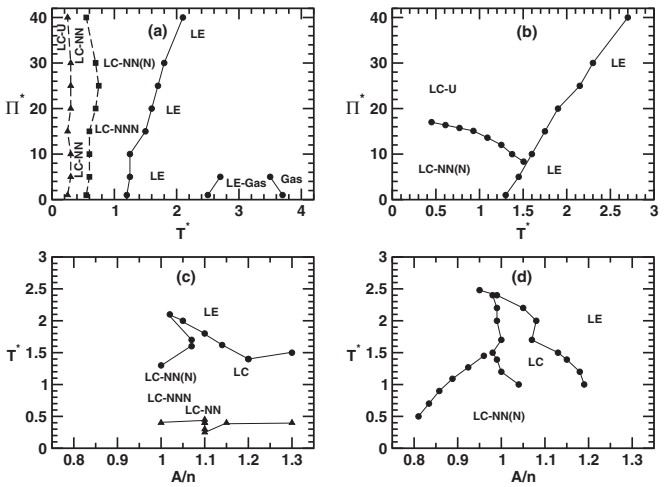

FIG. 6. The upper left panel shows the surface-pressure-versus-temperature phase diagram, whereas the lower left panel shows the temperature-versus-area-per-molecule phase diagram for system A. The upper and lower right panels show the corresponding phase diagrams for system B. These phase diagrams were estimated by analyzing the behavior of $\Psi_6, \mathcal{K}_{nn}, R_{xy}, \langle[\theta]\rangle, A/n$, and $(A/n)\langle\cos(\theta)\rangle$ for both systems.

specific heat at constant surface pressure were also estimated for some representative values of the surface pressure [57]. The Π^* versus T^* phase diagram is shown in Fig. 6(a) for system A. The LE-LC phase transition is located in the temperature interval $1.2 \leqslant T \leqslant 2.1$, and it rises almost linearly with an average slope of about 44.4. The coexistence of the subphases NN and NNN, denoted by NN(N), was obtained at relatively high surface pressures, $\Pi^* \approx 30$, and at intermediate temperatures, $0.7 \lessapprox T^* \lessapprox 1.8$. The NN subphase occurred for surface pressure values $\Pi^* \lessapprox 40$ in the low-temperature interval, $0.2 \lessapprox T^* \lessapprox 0.70$. In addition, the NNN subphase was obtained for $0 < \Pi^* < 15$, in the temperature interval $0.60 \lessapprox T^* \lessapprox 1.2$, and for higher pressure values it was found in the temperature interval $1.3 \lessapprox T^* \lessapprox 1.90$. In Fig. 6(b) the corresponding Π^*-versus-T^* phase diagram is plotted for system B. The LE-LC phase transition is located in the temperature interval $1.3 \leqslant T \leqslant 2.7$, and it rises almost linearly with an average slope of about 28.57, which is smaller than the one obtained for system A. Because of this, the LE-LC phase transition for system A shifts to lower temperatures as compared to the LE-LC phase transition for system B. In Figs. 6(a) and 6(b) the LE-LC phase coexistence line has been plotted with a continuous line and the estimated points are marked with (●). The locations of the subphases LC-NN and LC-NNN are plotted with (■) and (▲), respectively, and joined with segmented lines. The coexistence region LC-NN(N) is also represented with (▲). In in Figs. 6(c) and 6(d) the reduced temperature versus area per molecule phase diagrams are plotted for systems A and B, respectively. For system A the values of A/n are slightly higher than those attained for system B because of the long-range forces between the molecular heads. For system A the LC-NNN and LC-NN subphases occur in the interval $0.8 \leqslant A/n < 1.05$, with the former occurring at lower temperatures than the latter but at slightly higher temperatures as compared to system B. The LC-NN subphase occurs for $T^* < 0.5$ and appears to extend over the interval $1 \leqslant A/n \leqslant 1.3$. The LC-U phase is expected to occur at surface pressures $\Pi^* > 40$. From the above results one can state that as pressure increases, the LC-LE phase transition for system A shifts to lower temperatures and the location of the NN and NNN subphases also moves to smaller temperatures. Thus, the Coulomb interactions modify the structure and topology of the Π^*-versus-T^* and the T-versus-A/n phase diagrams and influence the stability of the phases. This is manifested in the shift of the phase coexistence lines to lower temperatures. These results are in qualitative agreement with experiments carried out in fatty acid monolayers with ionic head groups [45].

D. Isotherms and compressibility modulus

Let us begin this subsection by introducing two quantities that are important for the characterization of the system's mechanical properties. The first is the monolayer's compressibility, which is related to the behavior of the pressure versus area per molecule isotherms and is defined as $\kappa = -\frac{1}{A(dA/d\Pi)}$. Its inverse is known as the monolayer's area compression modulus, C_s^{-1}. A high value of C_s^{-1} indicates a monolayer's lower elasticity (rigid monolayer) and vice versa [19,63]. In Fig. 7 are plotted two surface-pressure-versus-area-per-molecule isotherms at temperatures $T^* = 0.5$ and $T^* = 1.5$, close to the LC-NN $\leftrightarrow$ LC-NNN and LE $\leftrightarrow$ LC phase transitions, respectively. These isotherms correspond to a monolayer with ionic molecular heads and were calculated for two system sizes, one with 144 (●) and the other with 256 (○) molecules. Their behavior looks very similar to the experimental isotherms: as pressure decreases the area per molecule increases and the higher the temperature the larger the area per molecule [45,64,65]. Note that at these two temperatures there appears to be no signature of a

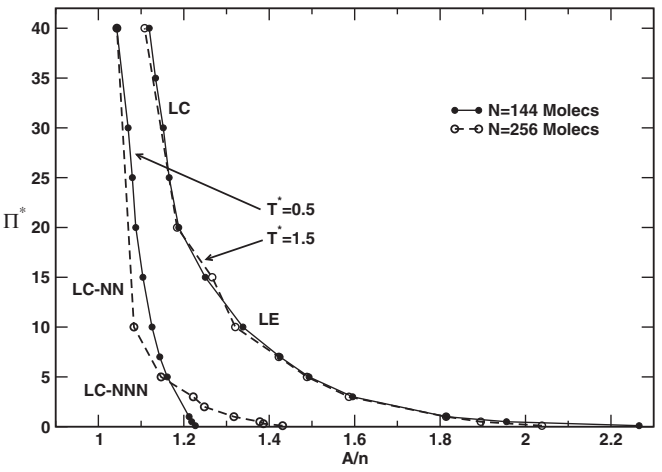

FIG. 7. Surface-pressure-versus-area-per-molecule isotherms for a monolayer with ionic molecular heads for systems with 144 and 256 molecules at $T^* = 0.5$ and $T^* = 1.5$. The high-temperature isotherm behavior for the two system sizes suggests that finite-size effects are negligible. On the contrary, the low-temperature isotherm behavior indicates that finite-size effects are non-negligible at low temperatures.

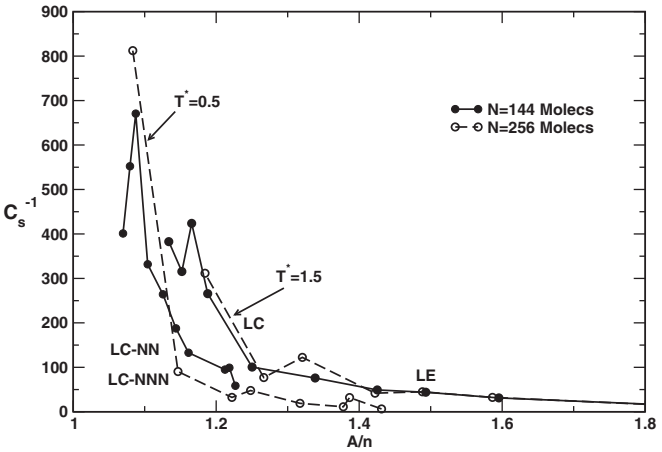

FIG. 8. Area compression modulus, C_s^{-1}, as a function of area per molecule for a monolayer with ionic molecular heads. This quantity was estimated from the surface pressure versus area per molecule isotherms shown in Fig. 7. The regions where the LE and LC phases as well as the LC-NN and LC-NNN subphases occur are indicated in the figure.

phase transition, that is, neither horizontal plateaus nor kinks are seen. To obtain these features one needs to perform extensive simulations on larger systems at nearby temperatures to locate the transitions; nonetheless, no effort was made to achieve this. Notwithstanding, the high-temperature isotherm behavior for the two system sizes suggests that finite-size effects are not significant. On the contrary, the low-temperature isotherm leads to higher values of C_s^{-1} for the larger system departing from the one corresponding to the small system. The increase in C_s^{-1} is more pronounced for $\Pi^* \leqslant 10$, suggesting that finite-size effects are non-negligible in the condensed phases. It is not surprising that the isotherms depend more on the system size since the isothermal compressibility modulus is the quantity that shows a discontinuity at a first-order phase transition or diverges at a second-order phase transition. In Fig. 8 the behavior of the monolayer's area compression modulus as a function of A/n is plotted at $T^* = 0.5$ and $T^* = 1.5$ and for the system sizes as indicated above. There one sees that the LE $\rightarrow$ LC phase transitions occurs at $A/n \approx 1.3$ and the values of C_s^{-1} are in the range $75 \lessapprox C_s^{-1} \lessapprox 120$. The transition LC-NN $\rightarrow$ LC-NNN takes place at about $A/n \approx 1.33$ and in this case C_s^{-1} is in the interval $25 \lessapprox C_s^{-1} \lessapprox 75$. These variation ranges for the monolayer's area compression modulus are consistent with the experimental intervals reported in Refs. [66,67]. In addition, the values of A/n are consistent with the values one can read in the temperature versus area per molecule phase diagram (see Fig. 6(c)]. From these results one can conclude that the LC-NNN phase is less rigid than the LC-NN phase.

At this point it is important to emphasize that the Monte Carlo simulations for a system with $N = 144$ molecules yields reliable results for single phases, as already noted above. However, finite-size effects are non-negligible in the LC phases and they may become important when LC-NN and LC-NNN phases coexist. To study in detail this phase coexistence one would need to simulate much larger systems and carry out a systematic finite-size analysis. Nonetheless, no attempt has been made to perform such an investigation.

V. CONCLUSIONS

We have carried out MC simulations in the N,Π,T ensemble of a CGMM of amphiphilic molecules deposited on a film. The molecular model incorporates the Coulomb interactions between the ions located at the center of the hydrophilic molecular heads. We investigated the interplay between the short-ranged van der Waals and Coulomb interactions between the molecular heads and its effect on the monolayer phase behavior. For small values of the surface pressure, $\Pi^* \leqslant 1$, and at high temperatures the area per molecule became large, $A/n > 5$, suggesting the existence of the gas phase. For surface pressures $\Pi^* \gtrapprox 1$, and in the temperature interval $2.5 < T^* < 3.7$, the coexistence between the LE and the gas phases was obtained as suggested by the values of A/n and the orientational correlation function, K_{nn}. The pure LE phase was obtained for $1 \leqslant \Pi^* \leqslant 40$ and $T^* < 2.5$, while the LC phase with its associated subphases, NN and NNN and their coexistence, NN(N), occurred for $T^* \lessapprox 2.1$ and for surface pressure values $\Pi^* < 30$. The LC-NN and LC-NNN subphases became apparent through the development of two maxima in the molecular tails average tilt angle, $\langle[\theta]\rangle$, that were obtained for most of the surface pressure values considered here. The former subphase occurring at lower temperatures, notwithstanding, the presence of these subphases was also manifested in the behavior of R_{xy} as two maxima for $\Pi^* \leqslant 10$. It was also found that the molecular tails oriented in such a way that they formed "vortex patterns" at temperatures in the interval, $0.5 < T^* < 1.5$, in between the two LC-NN and LC-NNN subphases and for intermediate pressures. These "vortex patterns" appeared to be stable for the two system sizes $N = 144$ and $N = 256$. However, a systematic finite-size analysis needs to be carried out to ascertain the stability of the patterns and the coexistence of the LC-NN and LC-NNN subphases. The low-temperature behavior of the order parameters Ψ_6 and R_{xy} suggest that the molecular heads undergo a reentrant disorder-order-disorder phase transition in the positions of the molecular heads and in the orientations of the molecular tails, respectively. In the ordered phase the molecular heads arrange to form a hexagonal lattice, whereas in the disordered phase they form a distorted polygonal lattice with four to six irregular sides. All these transitions are consistent with the behavior of the enthalpy and heat capacity at constant pressure as functions of temperature for the different values of the surface pressure [57]. More importantly, the shift of the LE-LC phase transition to smaller temperatures when the molecular heads carry an ion is in qualitative agreement with the experimental observations of fatty acid monolayer with ionic head groups [45]. We also calculated two isotherms at $T = 1.5$ and $T = 0.5$ for two system sizes $N = 144$ and $N = 256$ and found that their behavior looks very similar to the experimental isotherms [45,64,65]. From these isotherms we calculated the variation ranges of the monolayer's area compression modulus and encountered that they are consistent with the experimental values reported in Refs. [66,67]. Indeed, these area per molecule values were also consistent with the values one can read in the temperature-versus-area-per-molecule phase diagram. From the variation ranges of the monolayer's area compression modulus one can conclude that the LC-NNN is less rigid than the LC-NN.

ACKNOWLEDGMENTS

We acknowledge full financial support from DGAPA-UNAM under Contract No. IN-118410. C.G.C. also thanks support from CONACYT. We also thank the Condensed Matter group at Mainz lead by Professor Dr. F. Schmid for sharing with us their code for the simulations of the CGM of Langmuir monolayers with short-ranged interactions.

[1] M. Lösche, E. Sackmann, and H. Möhwald, Ber. Bunsen-Ges. Phys. Chem. **87**, 848 (1983).
[2] B. Moore, C. M. Knobler, D. Broseta, and F. Rendelez, J. Chem. Soc. Farad. Trans. **82**, 1753 (1986).
[3] C. M. Knobler, Science **249**, 870 (1990).
[4] B. G. Moore, C. M. Knobler, S. Akamatsu, and F. Rondelez, J. Phys. Chem. **94**, 4588 (1990).
[5] A. M. Bibo, and I. R. Peterson, Adv. Mater. **2**, 309 (1990).
[6] A. M. Bibo, C. M. Knobler, and I. R. Peterson, J. Chem. Phys. **95**, 5591 (1991).
[7] C. M. Knobler and R. C. Desai, Ann. Rev. Phys. Chem. **43**, 207 (1992).
[8] V. M. Kaganer, I. R. Peterson, R. M. Kenn, M. C. Shih, M. Durbin, and P. Dutta, J. Chem. Phys. **102**, 9412 (1995).
[9] B. Fischer, E. Teer, and C. M. Knobler, J. Chem. Phys. **103**, 2365 (1995).
[10] D. Vollhardt, Adv. Colloid Interface Sci. **64**, 143 (1996).
[11] I. Kuzmenko, V. M. Kaganer, and L. Leiserowitz, Langmuir **14**, 3882 (1998).
[12] A. Datta, J. Kmetko, A. G. Ritcher, C-J. Yu, and P. Dutta, Langmuir **16**, 1239 (2000).
[13] P. Dynarowicz-Latka, A. Dhanabalan, O. N. Oliviera, Jr., Adv. Colloid Interface Sci. **91**, 221 (2001).
[14] Z. Cai and S. A. Rice, Faraday Discuss. Chem. Soc. **89**, 211 (1990).
[15] F. Schmid and M. Schick, J. Chem. Phys. **102**, 2080 (1995).
[16] F. Schmid, Phys. Rev. E **55**, 5774 (1997).
[17] E. Ruckenstein and B. Li, J. Phys. Chem. **100**, 3108 (1996).
[18] V. B. Fainerman and D. Vollhardt, J. Phys. Chem. B **103**, 145 (1999).
[19] D. Vollhardt and V. B. Fainerman, Adv. Colloid Interface Sci. **127**, 83 (2006).
[20] V. B. Fainerman and D. Vollhardt, J. Phys. Chem. B **110**, 10436 (2006).
[21] N. Nandi and D. Vollhardt, Acc. Chem. Res. **40**, 351 (2007).
[22] J. Harris and S. A. Rice, J. Chem. Phys. **89**, 5898 (1988).
[23] J. P. Bareman, G. Cardini, and M. L. Klein, Phys. Rev. Lett. **60**, 2152 (1988).
[24] J. P. Bareman and M. Klein, J. Phys. Chem. **94**, 5202 (1990).
[25] S. Karaborni and S. Toxvaerd, J. Chem. Phys. **96**, 5505 (1992).
[26] S. Karaborni, Langmuir **9**, 1334 (1993).
[27] F. M. Haas, R. Hilfer, and K. Binder, J. Chem. Phys. **102**, 2960 (1995).
[28] F. M. Haas and R. Hilfer, J. Chem. Phys. **105**, 3859 (1996).
[29] F. M. Haas, R. Hilfer, and K. Binder, J. Phys. Chem. **100**, 15290 (1996).
[30] C. Stadler, H. Lange, and F. Schmid, Phys. Rev. E **59**, 4248 (1999).
[31] C. Stadler and F. Schmid, J. Chem. Phys. **110**, 9697 (1999).
[32] F. Schmid, C. Stadler, and H. Lange, Colloid. Surface. **149**, 301 (1999).
[33] Dominik Duchs, B.Sc. thesis, Johannes Gutenberg Universitat, 1999.
[34] D. Düchs and F. Schmid, J. Phys.: Condens. Matter **13**, 4853 (2001).
[35] F. Schmid, D. Düchs, O. Lenz, and C. Loison, *Computational Soft Matter: From Synthetic Polymers to Proteins*, Lecture Notes, NIC Series, Vol. 23, edited by Norbert Attig, Kurt Binder, Helmut Grubmüller, and Kurt Kremer (John von Neumann Institute for Computing, Jülich, 2004), pp. 323–346.
[36] Y. N. Kaznessis, S. Kim, and R. G. Larson, Biophys. J. **82**, 1731 (2002).
[37] S. O. Nielsen, C. F. Lopez, P. B. Moore, J. C. Shelley, and M. L. Klein, J. Phys. B **107**, 13911 (2003).
[38] S. Baoukina, L. Monticelli, S. J. Marrink, and D. P. Tielman, Langmuir **23**, 12617 (2007).
[39] R. L. McMullen and S. P. Kelty, J. Phys. Chem. B **111**, 10849 (2007).
[40] S. L. Duncan and R. G. Larson, Biophys. J. **94**, 2965 (2008).
[41] J. J. Giner-Casares, L. Camacho, M. T. Martin-Romero, and J. J. López Cascales, Langmuir **24**, 1823 (2008).
[42] Delara Mohammad-Aghaie, E. Macé, C. A. Sennoga, J. M. Sneddon, and F. Bresme, J. Phys. Chem. B **114**, 1315 (2010).
[43] H. Mantsch, S. F. Weng, P. W. Yang, and H. H. Eysel, J. Mol. Struct. **324**, 133 (1994).
[44] A. Datta, J. Kmetko, C. J. Yu, A. G. Ritcher, K. S. Chung, J. M. Bai, and P. Dutta, J. Phys. Chem. B **104**, 5797 (2000).
[45] R. Johann, D. Vollhardt, and H. Möhwald, Langmuir **17**, 4569 (2001).
[46] M. Yazdanian, H. Yu, and G. Zografi, Langmuir **6**, 1093 (1990).
[47] I. Watanabe, H. Tanida, and S. Kawauchi, J. Am. Chem. Soc. **119**, 12018 (1997).
[48] J. Kmetko, A. Datta, G. Evmenenko, and P. Dutta, Jour. Phys. Chem. B **105**, 10818 (2001).
[49] T. M. Bohanon, B. Lin, M. C. Shih, G. E. Ice, and P. Dutta, Phys. Rev. B **41**, 4846 (1990).
[50] M. C. Shi, T. M. Bohanon, J. M. Mikrut, P. Zschack, and P. Dutta, J. Chem. Phys. **96**, 1556 (1992).
[51] M. C. Shi, M. K. Durbin, and A. Malik, J. Chem. Phys. **101**, 9132 (1994).
[52] G. Ma, and H. C. Allen, Langmuir **22**, 5341 (2006).
[53] JEfrosini Kokkoli, and Charles F. Zukoski, Langmuir **16**, 6029 (2000).
[54] K. Thirumoorthy, N. Nandi, and D. Vollhardt, Jour. Phys. Chem. B **109**, 10820 (2005).
[55] K. Thirumoorthy, N. Nandi, and D. Vollhardt, Langmuir **23**, 6991 (2007).
[56] C. B. George, M. A. Ratner, and I. Szleifer, J. Chem. Phys. **132**, 14703 (2010).

[57] See Supplemental Material at http://link.aps.org/supplemental/10.1103/PhysRevE.91.032409 for the behavior of the entalphy and specific heat as functions of temperature for some representative values of the surface pressure.
[58] G. Weidemann, G. Brezesinski, D. Vollhardt, F. Bringezu, K. de Meijere, and H. Möhwald, J. Phys. Chem. B **102**, 148 (1998).
[59] D. Frenkel and B. Smit, *Understanding Molecular Simulation: From Algorithms to Applications*, 2nd ed. (Academic Press, London, 2002).
[60] F. Figueirido, G. Del Buono, and R. M. Levy, J. Chem. Phys. **103**, 6133 (1995).
[61] V. Ballenegger, A. Arnold, and J. J. Cerd, J. Chem. Phys. **131**, 094107 (2009).
[62] J. S. Hub, B. L. de Groot, H. Grubmüller, and G. Groenhof, J. Chem. Theor. Comput. **10**, 381 (2014).
[63] F. Behroozi, Langmuir **12**, 2289 (1996).
[64] O. Albretch, H. Matsuda, and K. Eguchi, Colloid. Surface. A **284-285**, 166 (2006).
[65] P. Ganguly and D. V. Paranjape, Langmuir **13**, 5433 (1997).
[66] J. Davies and E. K. Rideal, *Interfacal Phenomena*, 2nd ed. (Academic Press, New York, 1963).
[67] G. Capuzzi, P. Lo Nostro, K. Kulkarni, and J. Fernandez, Langmuir **12**, 3957 (1996).